2009

Exploring the Transition from Wall Slip to Bulk Shearing Banding in Well-Entangled DNA Solutions

Shi-Qing Wang, *University of Akron*
Pouyan E. Boukany, *University of Akron Main Campus*

Exploring the transition from wall slip to bulk shearing banding in well-entangled DNA solutions

Pouyan E. Boukany and Shi-Qing Wang*

Received 20th March 2008, Accepted 17th October 2008
First published as an Advance Article on the web 15th December 2008
DOI: 10.1039/b804791j

In this study we have carried out a combination of rheometric and particle-tracking velocimetric (PTV) measurements to investigate nonlinear rheological behavior of three entangled DNA solutions (with *ca.* 150 entanglements per chain) and, in particular, to explore a transformation from slip-dominated steady-state flow to bulk shear inhomogeneity. In the stress plateau regime, an elastic recoil-like response occurs transiently at either interfaces or sample interior after stress overshoot during a startup shear. In both startup shear and creep mode, wall slip, bulk shear banding or a combination of both have been observed in both transient and steady states. The water-based solution shows massive wall slip allowing the bulk to remain in the Newtonian flow regime. Use of glycerol as a solvent can effectively reduce interfacial slip, permitting bulk shear banding to develop in both controlled-rate and controlled-stress modes. For the glycerol based solution, a sufficiently high Weissenberg number can attain in the rheometer where PTV observations reveal homogenous shear in steady state.

1. Introduction

Soft matter encompasses a variety of structured materials from colloids, polymers, liquid crystals, micelles, foams, gels, emulsions to membranes. Visible viscoelasticity arises from the organization of and interactions among the constituents. For short time scales (relative to the longest relaxation dynamics) when such a matter exhibits apparent elasticity, one may wish to inquire about the cohesion of such a transient solid. All solids have finite strength and cannot undergo external deformation indefinitely without cohesive failure. This means, for viscoelastic materials, that cohesive breakdown may occur as an external deformation is continually imposed over a time scale, for which the materials may be regarded as quasi-elastic solids. Extensive reviews have discussed many aspects of various complex fluids including rheological behavior without emphasis on the role of material elasticity in the case of entangled polymers.[1,2]

The shear flow behavior of entangled polymers is an important subject in soft condensed matter physics because of the wide-ranged applications of these materials. Grocery bags, drink bottles, disposable plates, synthetic fibers (polyester clothing) and many micro-fabrications in electronic and optical communication industries all involve subjecting polymeric liquids to flow. These polymeric liquids are rather difficult to study rheologically for two reasons: well-entangled solutions are (a) typically too stiff to avoid edge instability and (b) tend to suffer interfacial wall slip. One polymer like system that does not encounter these experimental challenges is a wormlike micellar solution whose nonlinear rheological behavior has been extensively investigated in the past fifteen years or so both experimentally[3–14] and theoretically.[15–18] In particular, the extreme shear thinning character corresponding to a stress plateau[19] has been explored and shown to be associated with shear banding. Three recent reviews[20–22] have surveyed most experimental and modeling activities on shear banding of micellar solutions. However, it has been clear in the community that shear banding in wormlike micellar solutions cannot be taken to suggest shear banding in polymer solutions. Due to their ability to self-assemble and to adjust the micellar length at a given concentration through either coagulation or breakup, wormlike micelles could shear band in ways that polymers cannot. Associating polymer solutions[23,24] and colloidal glasses[25] are two other examples capable of shear banding without chain disentanglement.

Overcoming the experimental difficulties indicated above and inspired by the notion of a yield-like transition associated with shear thinning of well-entangled polymeric liquids, recent particle-tracking velocimetric (PTV) observations finally revealed inhomogeneous deformation in startup shear,[26] large-amplitude oscillatory shear[27] and non-quiescent relaxation after large step strain[28] in various entangled polybutadiene (PBD) solutions. It appears obvious to us that the temporary network due to chain entanglement is actually of finite cohesive strength and can suffer inhomogeneous collapse at large external deformations.[29] A subsequent independent PTV study also observed transient shear banding in startup shear of moderately entangled solutions.[30]

DNA solutions appear to be good model systems for studying the shear thinning behavior of entangled polymers made of chemically bonded chains (in contrast to micelles due to self-assembly). Since their elastic plateau modulus can be as low as 50 Pa, rheological complications such as edge fracture can be avoided in a conventional cone–plate setup, and steady state shear is readily accessible,[31] in contrast to polymeric liquids. In the present work, a combination of particle-tracking velocimetric (PTV) and *in situ* conventional rheometric measurements were carried out to investigate the relationship between wall slip and internal shear banding, *e.g.*, when wall slip is important and when shear banding is dominant. In particular, we will show that

Department of Polymer Science, University of Akron, Akron, Ohio 44325, USA. E-mail: swang@uakron.edu

these well entangled fluids may yield like soft solids at the either interface or in the bulk in both controlled-rate and stress shear mode, depending on their intrinsic magnitude of wall slip.

2. Experiment

2.1. Materials

In this work we study well entangled solutions made of linear double strand DNA calf thymus. The highly purified (dehydrated) DNA with a weight-average molecular weight of $N = 7.5 \times 10^4$ bp (base pair) was purchased from USB Co. At a constant concentration of $C = 22.0$ mg mL^{-1}, three solutions were prepared with water, ethylene glycol (ETG) and glycerol as the solvent respectively. Following a previous study,[32] to eliminate electrostatic effects, NaCl is introduced to screen the negative charge of the DNA backbone and achieve a θ solution. An aqueous buffer was first made, comprised of 10 mM Tris-HCl (pH 7.9), 0.8 mM ethylene diamine tetraacetic acid (EDTA) (which prevents degradation) and 20 mM NaCl. Then an appropriate amount of dehydrated DNA was dissolved in it by gentle stirring to make the water-based solution. To prepare the other two solutions, a calculated amount of dry DNA and suitable amount of either ETG or glycerol were first introduced into the buffer and mixed gently, where the initial weight ratio of water to ETG or glycerol is around one. Then, the water was allowed to evaporate for several days. The final sample has about 1–2% residual water. To inhibit degradation, the DNA solutions are stored in refrigerator at $T \simeq 4$ °C after water evaporation. Silver-coated particles (Dantec Dynamic HGS-10) were introduced during the sample preparation at a low concentration (around 300 ppm) for tracking the velocity profile.

2.2 Rheometric and particle-tracking velocimetric (PTV) measurement

Rheological and PTV measurements were carried out using a Physica MCR-301 rotational rheometer (Anton Paar) in a cone–plate setup, all at room temperature around 23 °C. For conventional rheometric measurements, a cone of angle 2° and diameter 25 mm is employed. To prevent water evaporation in the water solution during rheological measurements, the meniscus of the aqueous DNA solution in the cone-plate cell was surrounded by a low-molecular weight poly(dimethyl siloxane). To enable PTV observations, a sheet of laser passes across the sample thickness from the stationary plate that is made of glass and a CCD camera captures movements of the illuminated particles onto a VCR. To eliminate reflections of the illuminating laser, both flat (smooth) metallic cone and plate surfaces were coated with a thin layer of black enamel (Rust-oleum Corporation, specialty high heat black enamel), where a small window on the glass plate is left clear of any paint. To study the surface roughness effect, black-painted sandpapers [Virginia Abrasive, USA, (240 grit, #4687A13)] were glued to the cone and plate. To observe the flow field inside the sample, a flexible transparent film with diameter around 27 mm is wrapped around the meniscus of a cone–plate assembly of 4° cone angle and 25 mm diameter, as depicted in Fig. 1. The sample was filled up to the film for PTV measurements. Our observation plane is 3–4 mm from the meniscus.

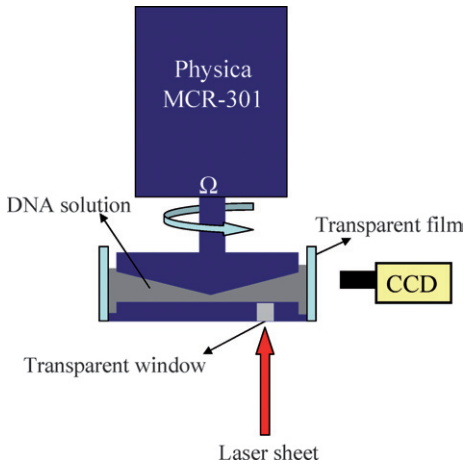

Fig. 1 A depiction of the PTV set up in cone–plate shear cell, where a laser sheet illuminates across the sample thickness, and the moving particles are filmed by a CCD camera mounted with an objective lens. The transparent wall is 1–2 mm away from outer edge of the cone. The observation plane is 3–4 mm from the meniscus.

3. Results and discussions

3.1. Conventional rheometric measurements

3.1.1 Linear viscoelasticity. Fig. 2 shows storage and loss moduli G' and G'' at a concentration of $C = 22$ mg mL^{-1} in water, ETG and glycerol respectively from small amplitude oscillatory shear (SAOS) measurements. The inset in Fig. 2 displays approximate overlapping of G' and G'' against the normalized frequency $\omega\tau$, suggesting that the level of chain entanglement is nearly the same in these three solutions although the different solvents are expected to produce different levels of counterion condensation and affect the coil size. At this point, it is not obvious why the onset entanglement molecular weight M_e appears to be the same for these three solutions. Since M_e is correlated with the packing length p, perhaps this result can be taken to suggest that p of a DNA chain, which is a measure of the

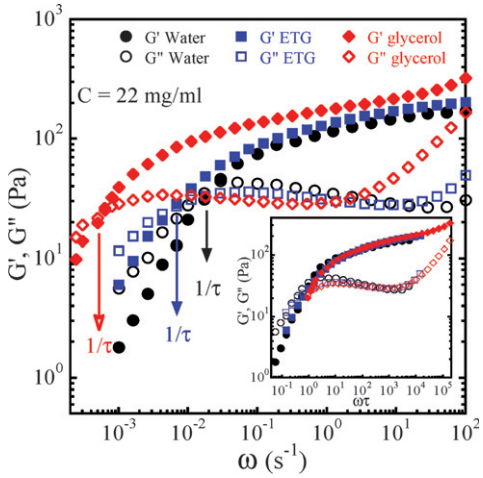

Fig. 2 Storage G' and loss G'' moduli *versus* a frequency ω for 22 mg mL^{-1} of DNA in water, ETG and glycerol. The inset shows changes G' and G'' as a function of normalized frequency ($\omega\tau$).

Table 1 Characteristics of 22 mM mL^{-1} entangled DNA solutions

Solvent	G_p/Pa	M_e/g mol^{-1}	M_w/M_e	τ/s	$\tau_R = \tau/3Z$/s
100% Water	166.23	0.32×10^6	156	56	0.118
98% ETG–2% water	173	0.313×10^6	159	145	0.302
98% Glycerol–2% water	169	0.32×10^6	156	1900	4.06

chain thickness perpendicular to the backbone,[33] is not much different in the three different solvents. The characteristics of these samples based on the SAOS measurements are listed Table 1, where the plateau modulus G_p was estimated from the value of G' at the frequency where G'' shows a minimum, and the terminal relaxation time τ is estimated from the inverse of the crossover frequency where $G' = G''$, and M_e is estimated by $M_e = CRT/G_p$, where C, R and T are the concentration, gas constant and temperature respectively. The number of entanglement is given by $Z = M_w/M_e$. The Rouse time is estimated by $\tau_R = \tau/3Z$.

3.1.2. Interfacial slip and beyond. When entangled fluids are sandwiched between two solid surfaces, an interfacial layer is created between adsorbed chains and unbounded free chains. There have been various examples in simple shear of polymeric entangled solutions[34–36] and melts[37–41] that show wall slip due to deformation-induced interfacial disentanglement. The slip due to loss of entanglement at the interface can be quantitatively described according to the following formula for the Navier–de Gennes extrapolation length b

$$b = (\eta_{bulk}/\eta_i)a_L \quad (1)$$

The maximum level of slip can be estimated by taking the zero-shear viscosity in the Newtonian flow regime as η_{bulk} and the solvent viscosity η_s as the lower bound of the interfacial viscosity η_i in the slip layer. For η_s, we would have 1×10^{-3}, 2.3×10^{-2} and 7.5×10^{-1} Pa s for water, ETG and glycerol respectively. Table 2 lists three values of $b_{max} = (\eta_{bulk}/\eta_s)a_L$ for the three solutions, where we use the same value for a_L as an approximation.[31] The geometrical significance of the slip length b can be visualized from Fig. 3 for simple shear. When the system is sheared beyond the terminal flow (Newtonian) regime, *i.e.*, when the imposed V is such that $(V/H)\tau > 1$, *i.e.*, $V > V_c = H/\tau \equiv H\dot{\gamma}_c$, wall slip will take place. For each increasing value of $V > V_c$, the system can accommodate the moving surface by wall slip without necessarily undergoing higher bulk deformation as depicted in Fig. 3: $V - V_c = 2V_s$, while keeping the stress relatively constant at $\sigma \simeq \eta_{bulk}\dot{\gamma}_c \simeq G_p$, *i.e.*, stress plateau like behavior could be expected, where $\eta_{bulk} \simeq G_p\tau$. The maximum $V_{s(max)}$ that the solution can display is given by $b_{max}\dot{\gamma}_c = b_{max}/\tau$ according to Fig. 3 and is listed in

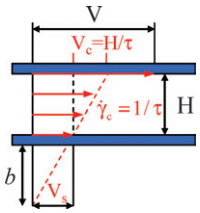

Fig. 3 A depiction of wall slip in simple shear in the stress plateau, where the slip length, also known as the Navier–de Gennes extrapolation length b characterizes the effect of interfacial slip in terms of the slip velocity V_s and true shear rate V_c/H such that $b = (V_s/V_c)H$ and $V = V_c + 2V_s$ if symmetric wall slip occurs.

Table 2. Thus, the imposed shear rate $\dot{\gamma}$ or the Weissenberg number $Wi = \dot{\gamma}\tau$, can be as high as $\dot{\gamma}_{sb} = V_{sb}/H = \dot{\gamma}_c + (2b_{max}/H)/\tau$, or Weissenberg number $(Wi)_{sb} = \dot{\gamma}_{sb}\tau$ may be as high as $(1 + 2b_{max}/H)$ before chain disentanglement has to take place away from the interfacial layer, where the subscript "sb" stands for the borderline between slip to bulk failure. Table 2 listed the value of $(Wi)_{sb}$ by taking $H \simeq 1$ mm. To reduce wall slip and the value of $(Wi)_{sb}$, we can decrease the viscosity ratio in eqn (1). Since the viscosity of an entangled solution typically increases more slowly than linearly with the solvent viscosity, b can be reduced by a choice of solvent other than water of such low viscosity.

3.1.3. Nonlinear rheology. We employed both startup shear (controlled rate) and creep (controlled stress) modes to investigate the rheological responses of the three DNA solutions. Fig. 4(a) to 4(c) show the shear stress growth as a function of the elapsed strain at various apparent rates. All three solutions show stress overshoot beyond the terminal regime and additional undershoot at sufficiently high rates. In contrast to well entangled polymer solutions where it is challenging to achieve steady state due to edge fracture,[42] our measurements attain steady state with little experimental complications such as edge fracture thanks to the softness of these solutions.

Fig. 5(a) to (c) show rises of the apparent shear rate $\dot{\gamma}$ as function of strain in creep for the three DNA solutions. It seems that more strain units are required to reach steady-state value in the controlled-stress mode than in the controlled-rate mode, and at a higher applied stress. The gradual rise in the apparent shear rate is observed without any discernible edge fracture in these creep measurements. Negligible changes in G' and G'' were found before and after startup shear and creep measurements in steady state. For example, linear viscoelastic measurements following steady shear show that there is negligible edge instability to cause any sample loss and to produce any irrecoverable reduction in $|G^*|$.

Finally, the steady state values of σ and $\dot{\gamma}$ from both startup shear and creep measurements form two flow curves in Fig. 6

Table 2 The interfacial slip and other characteristics of entangled DNA solutions

Solvent	$\eta_{bulk} \times 10^3$	η_s	b_{max}/mm	$\dot{\gamma}_c$	$(Wi)_{sb} = 2b_{max}/H$	$V_{s(max)}$/mm s^{-1}
100% water	5.8	0.001	737	0.018	1472	13
ETG : water (98 : 2)	13	0.023	71	0.0068	142	0.5
glycerol : water (98 : 2)	58	0.7	11	0.0005	21	0.0055

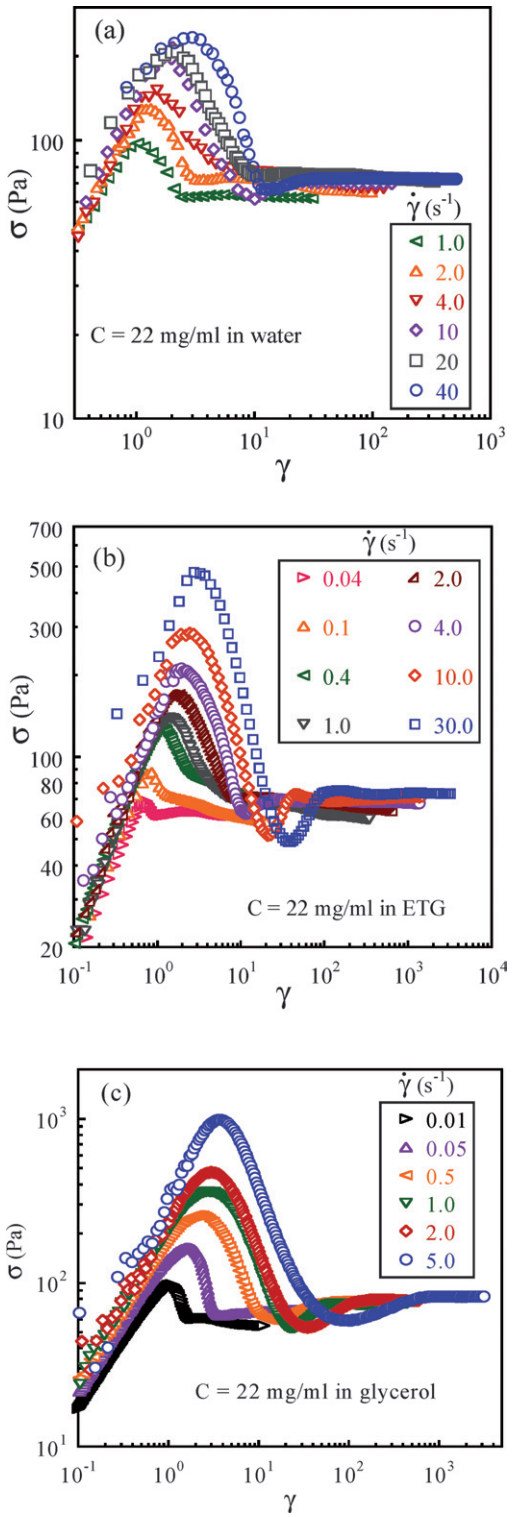

Fig. 4 The shear stress σ as a function of the elapsed strain $\gamma(t) = \dot{\gamma}t$ during startup shear at different imposed rates for the three solutions in (a) water, (b) ETG, and (c) glycerol.

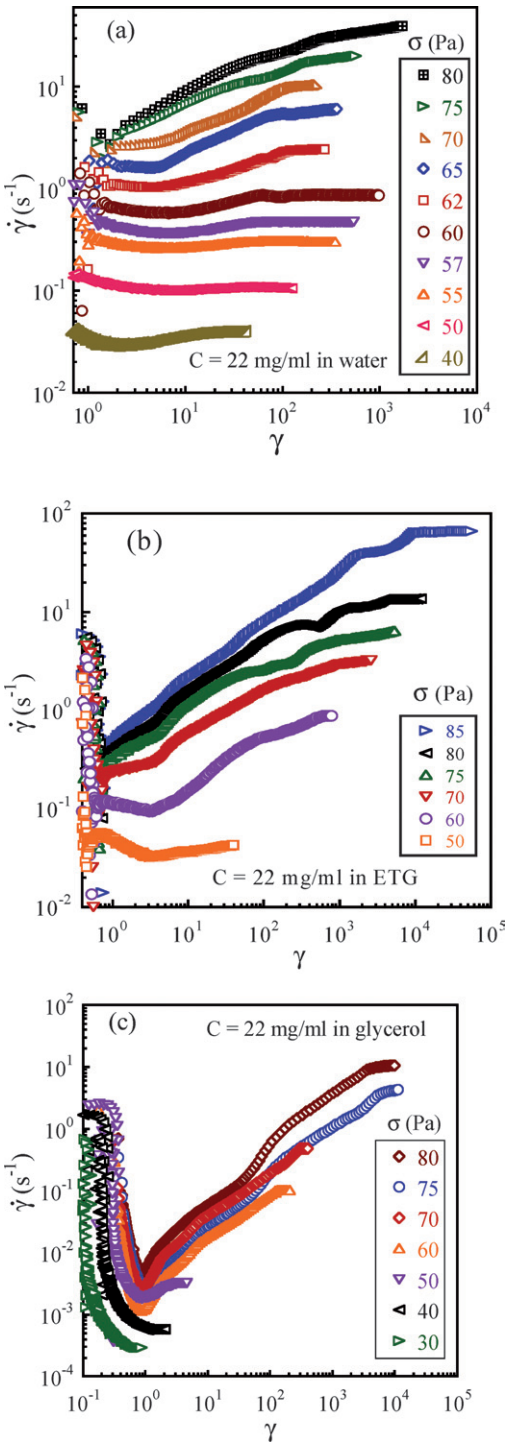

Fig. 5 The rise of the apparent shear rate $\dot{\gamma}$ as a function of $\gamma(t) = \int_0^t \dot{\gamma}(t')\mathrm{d}t'$ in discrete creep experiments at various applied σ for the three solutions in (a) water, (b) ETG, and (c) glycerol.

both of which are considerably below the curve obtained from oscillatory shear measurements of $|G^*|$ *vs.* ω and overlap well, which is consistent with a previous report on steady state flow curves of entangled polymer solutions.[42]

3.2. PTV measurements of transient and steady states

3.2.1. Homogenous flow in terminal regime. At low shear rates with $\dot{\gamma}\tau < 1$, there is no stress overshoot during startup shear. Fig. 7(a) and (b) confirm for both water and ETG based

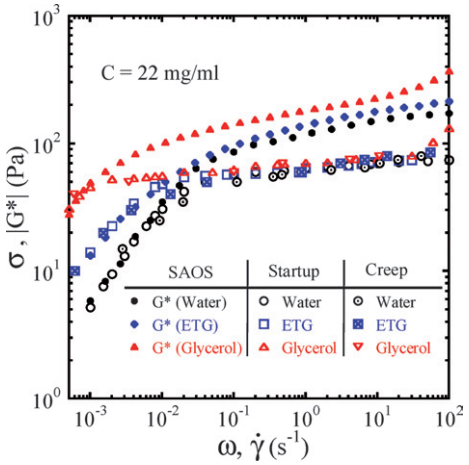

Fig. 6 Flow curves of the three solutions according to small amplitude oscillatory shear (SAOS), startup shear, and creep measurements.

solutions that the velocity profile is uniform across the sample thickness Y at all times during shear. These results are consistent with earlier reports[26] of homogeneous shear in entangled polymer solutions in the terminal flow regime.

3.2.2. Wall slip during startup shear. Beyond the terminal regime, stress overshoot emerges upon startup shear. Fig. 8(a) and (b) display the time-dependent velocity profile during startup shear of the DNA solutions at applied rates of 1.0 and 4.0 s^{-1} respectively. Before the stress overshoot, the velocity profile is linear across the gap. After the shear stress maximum, strong failure occurs close to the interfaces, especially at the upper moving surface. As long as the corresponding Weissenberg number is lower than $(Wi)_{sb}$ listed in Table 2, this failure is probably due to chain disentanglement at the sample–wall interface leading to massive wall slip although our PTV technique does not have the required spatial resolution to confirm this assertion.

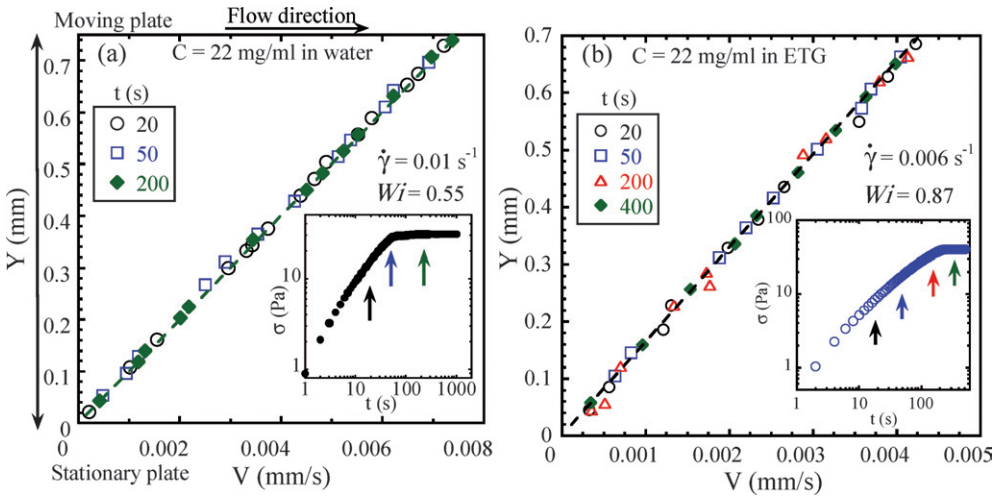

Fig. 7 PTV measurements of velocity profile at different times during startup shear in the terminal flow regime with (a) $\dot{\gamma} = 0.01\ s^{-1}$ for water-based solution. (b) $\dot{\gamma} = 0.006\ s^{-1}$ for the ETG-based solution. The insets show the time-dependent stress growth without stress overshoot.

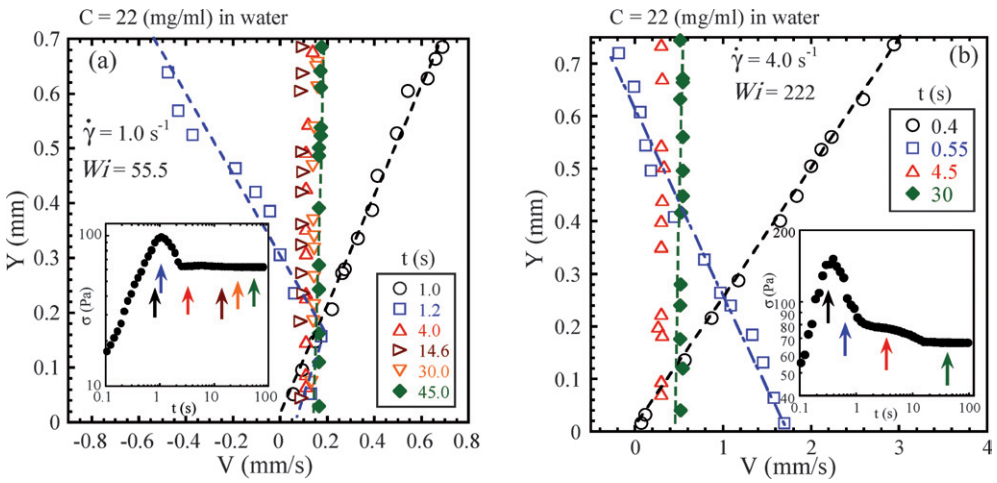

Fig. 8 PTV measurements of velocity profile at different times during startup shear with (a) $\dot{\gamma} = 1.0\ s^{-1}$ and (b) $\dot{\gamma} = 4.0\ s^{-1}$ for the water-based solution. The insets show time-dependent shear stress at the imposed shear rates.

Two remarks are in order. First, interfacial failure as revealed here by PTV observations usually precedes any bulk failure. Second, as anticipated by the discussion in section 3.1.2, the comparison between Fig. 8(a) and 8(b) shows that the increase in the applied velocity of the upper surface by a factor of four is completed "absorbed" by an increase in the magnitude of wall slip. In other words, referring to Fig. 3, the increase of V by a factor of 4 simply led to a rise in V_s by the same factor, corresponding to increased disentanglement at the interfaces. This is reasonable because the imposed V/H only corresponds to Weissenberg numbers $\ll (Wi)_{sb} = 1472$. Since $(Wi)_{sb}$ is proportional to $2b/H$ and b in eqn (1) is proportional to the bulk viscosity η_{bulk}, the present sample has an even wider range than a previous solution[31] of concentration $C = 10$ mg mL^{-1}, where wall slip is dominant, from $Wi > 1$ to $(Wi)_{sb} \simeq 1472$.

3.2.3 Shear banding (bulk failure) during startup shear for $Wi > 2b_{max}/H$. According to the information in Table 2, for significant shear banding to take place in the bulk in the water based solution, the plate velocity V needs to be in excess of $2V_{s(max)} \simeq 26$ mm s^{-1}. Unfortunately, our current PTV technique is accurate only for velocity values below 10 mm s^{-1}, making it difficulty to determine whether severe shear banding occurs in such entangled solutions.

As discussed in section 3.1.2 and presented in Table 2, the amount of slip is dramatically reduced by changing the solvent from water to glycerol, giving us a better chance to explore bulk shear inhomogeneity. When the imposed velocity $V > 2b_{max}/\tau$, *i.e.*, $V > 2V_{s(max)}$, or $\dot{\gamma}\tau > (Wi)_{sb} = 2b_{max}/H$, according to the subsection 3.1.2, the entanglement network can no longer maintain bulk flow in the terminal regime. Once the bulk flow is brought into the shear thinning regime, we have a chance to determine whether these entangled solutions would suffer the fate of inhomogeneous shear. For the ETG based solution, $2V_{s(max)} \simeq 1.0$ mm s^{-1} according to Table 2. Thus, a shear rate $V/H = 5$ s^{-1} should have brought the system well beyond the

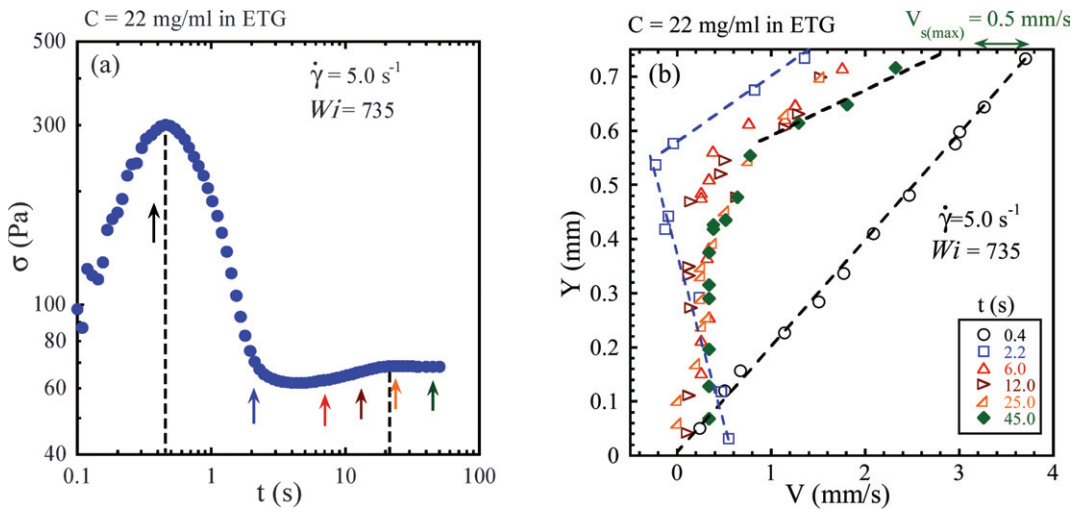

Fig. 9 (a) The time-dependent shear stress at $\dot{\gamma} = 5.0$ s^{-1}, for the ETG-based solution. (b) The corresponding velocity profiles at different times, where the maximum theoretically allowed magnitude of the slip velocity $V_{s(max)}$ is indicated.

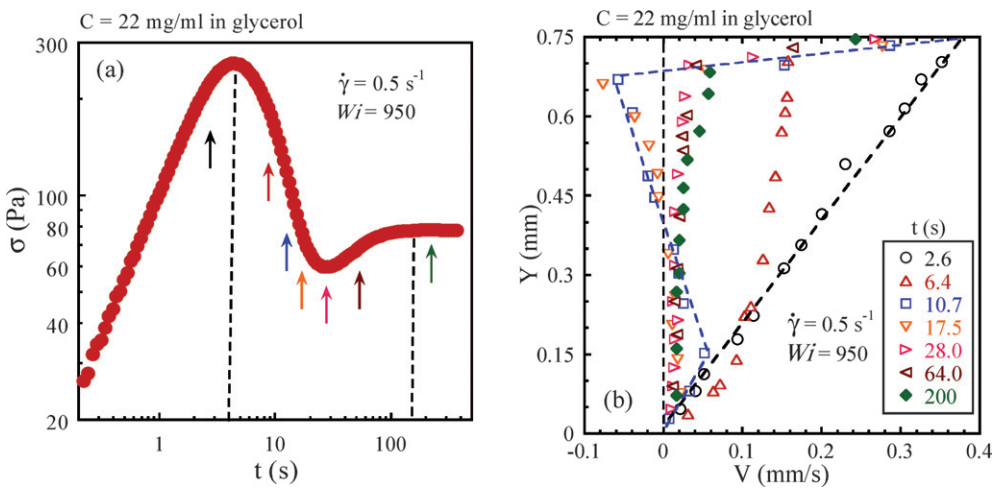

Fig. 10 (a) The time-dependent shear stress at $\dot{\gamma} = 0.5$ s^{-1}, for the glycerol-based solution. (b) The corresponding velocity profiles at different times.

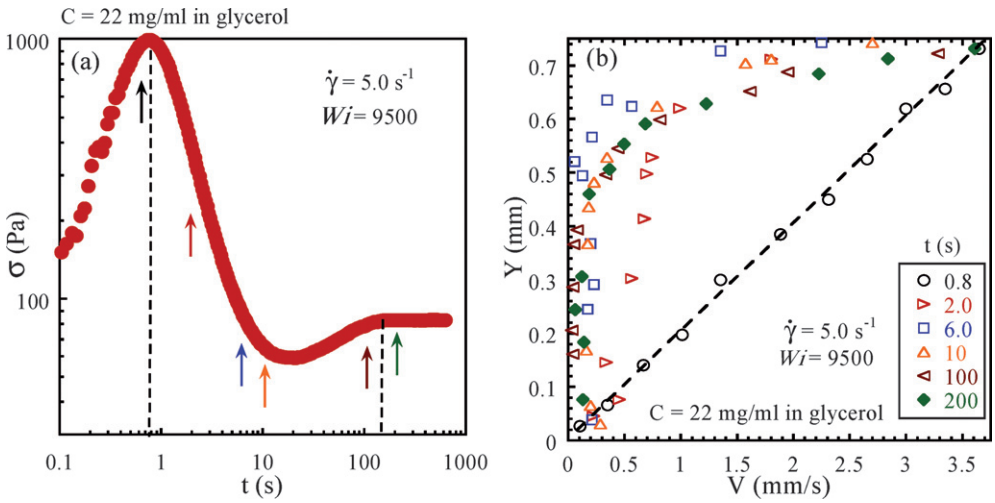

Fig. 11 (a) The time-dependent shear stress at $\dot{\gamma} = 5.0\ s^{-1}$, for the glycerol-based solution. (b) The corresponding velocity profiles at different times.

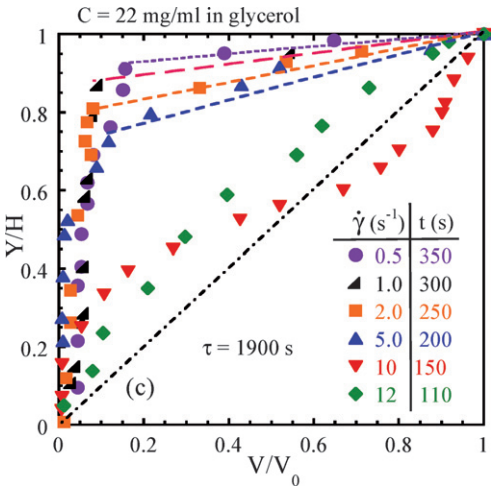

Fig. 12 Normalized steady state velocity profiles at different applied rates for the glycerol-based solution.

borderline between interfacial slip and bulk failure. Fig. 9(a) shows the shear stress as a function of time, and Fig. 9(b) presents the PTV determination of the flow profiles at different times. Indeed, significant shear banding is now visible in the sample interior.

For the glycerol based solution, $2V_{s(max)} \simeq 0.011$ mm s^{-1} according to Table 2. Thus, a shear rate of 0.5 is more than sufficient to allow shear banding. Fig. 10(a) and (b) and Fig. 11(a) and (b) show the transient behavior of the glycerol based solution during startup shear at two high rates. The velocity profiles are uniform across the gap till stress maximum. In each case from Fig. 9 to Fig. 11, internal failure took place to produce the stress undershoot. In the steady state, permanent shear banding prevails in these entangled solutions. At intermediate rates, interfacial slip is a visible component of the overall shear inhomogeneity as shown in Fig. 9(b). Finally, we summarize in Fig. 12 the adjustment of the steady-state velocity profiles as the imposed shear rate increases. At the highest rate of 12 s^{-1},

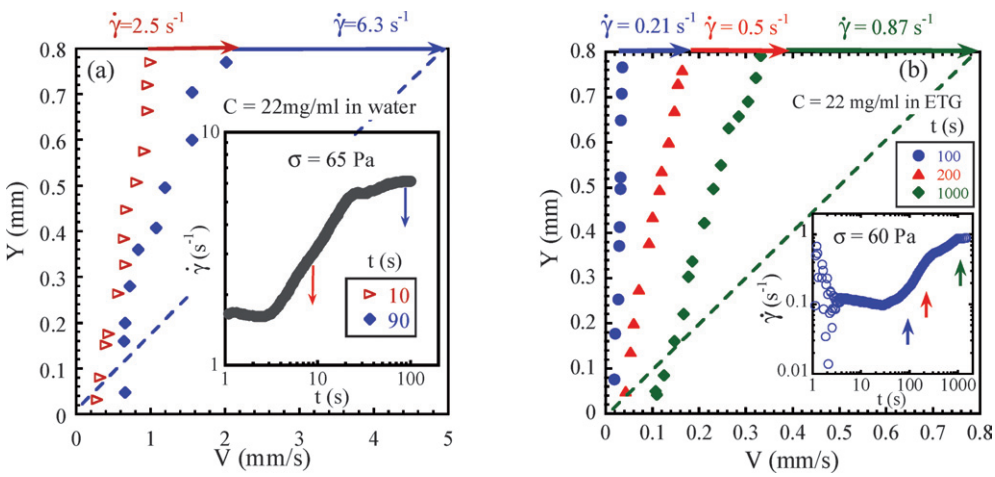

Fig. 13 The time-dependence of the velocity profile in the creep mode at (a) $\sigma = 65$ Pa for the water-based solution and (b) $\sigma = 60$ Pa for the ETG-based solution.

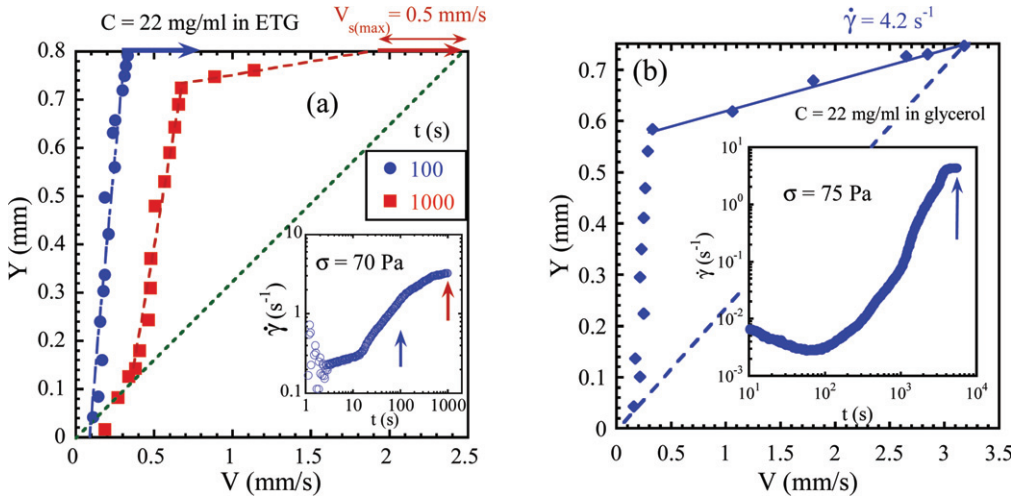

Fig. 14 The time-dependence of the velocity profile in the creep mode at (a) $\sigma = 70$ Pa for the ETG-based solution, where the maximum theoretically allowed magnitude of the slip velocity is indicated. (b) The steady state velocity profile at $\sigma = 75$ Pa for the glycerol-based solution where inset shows the rise of $\dot{\gamma}$ as a function of time.

corresponding to a Weissenberg number *Wi* as high as 22 800, the shear field turns nearly homogeneous, as expected.

3.2.4. Wall slip and shear banding in creep mode. Fig. 13(a) and (b) display the transient behavior of the water and ETG-based solutions under constant shear stress of 65 and 60 Pa respectively. The PTV measurements reveal dominance of wall slip. In neither case, the slip velocity has exceeded the maximum values listed in Table 2. It is plausible that the rise in the apparent rate originates from the increasing magnitude of wall slip.

At higher shear stresses, the resulting velocity would exceed $2V_{s(max)}$ such that the bulk is expected to undergo flow beyond the terminal regime and shear banding may be visible. In the ETG based solution, Fig. 14(a) shows interesting development of the velocity profile: in response to the shear stress of 70 Pa, the system initially displays a maximum amount of wall slip before the "erosion of chain entanglement" invades into the sample interior. In steady state, there is a combination of full interfacial slip and shear banding in the bulk. Fig. 14(b) shows the velocity profiles in the steady state for $\sigma = 75$ Pa in the glycerol based solution. Since the final rate corresponds to *Wi* equal to 7980, far greater than $(Wi)_{sb} = 21$, only bulk shear banding is evident from Fig. 14(b).

3.2.5 Comparison between controlled rate *vs.* controlled stress. Finally, we apply PTV to explore whether entangled liquids would respond differently depending on the mode of shear, *i.e.*, rate-controlled *vs.* stress-controlled. The rate-controlled shear prescribes a specific experimental time scale, *i.e.*, the reciprocal shear rate that determines how fast the initial external deformation is being imposed globally on the system, whereas the creep experiment, on the other hand, allows the system to find its own natural rates of shear over time. Although the two modes produce the same steady state values of the shear stress and apparent rate as shown in the inset of Fig. 15, our PTV observations reveal in Fig. 15 that different velocity profiles resulted. In particular, imposing a sudden velocity leads to a maximum

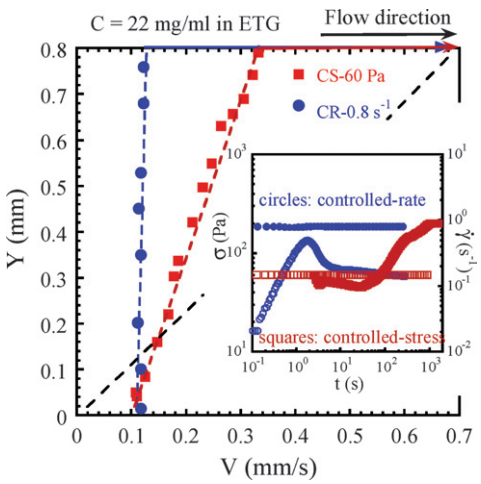

Fig. 15 Comparison of the velocity profiles during startup shear between rate-controlled and stress-controlled modes for the ETG-based solution, where the inset shows that both modes produce the same final apparent values of shear stress and rate.

level of wall slip, allowing the bulk to flow in the terminal regime, as shown by the circles in Fig. 15.

3.2.6 Comparison between interfacial slip *vs.* bulk failure. It has been reported that surface roughness could suppress wall slip.[43] For our water-based solution that is capable of massive wall slip, our PTV method should allow us to determine how surface roughness introduced by sandpapers alters the flow field. Fig. 16(a) and (b) show that the stress overshoot is stronger in presence of the surface roughness although the PTV observations do not have sufficient spatial resolution to detect any difference in steady state. At a low enough rate, it is possible that the interfacial slip simply becomes internal slip due to the surface roughness, *i.e.*, the failure still involves disentanglement of one monolayer of chains at the sandpaper. The effect of surface roughness is

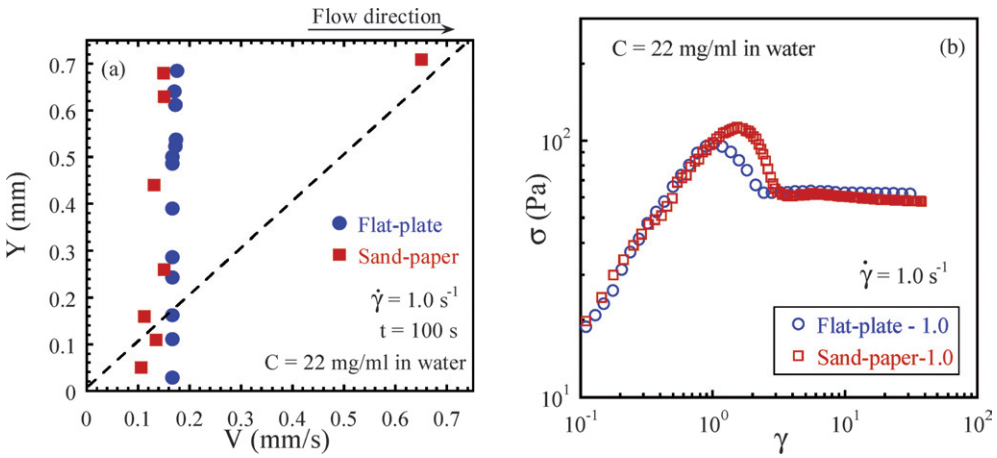

Fig. 16 (a) PTV observations at apparent shear rate 1 s^{-1} showing little difference between the flat surfaces and sandpaper surfaces, (b) where the rheological measurements of the stress overshoot do indicate a marked difference.

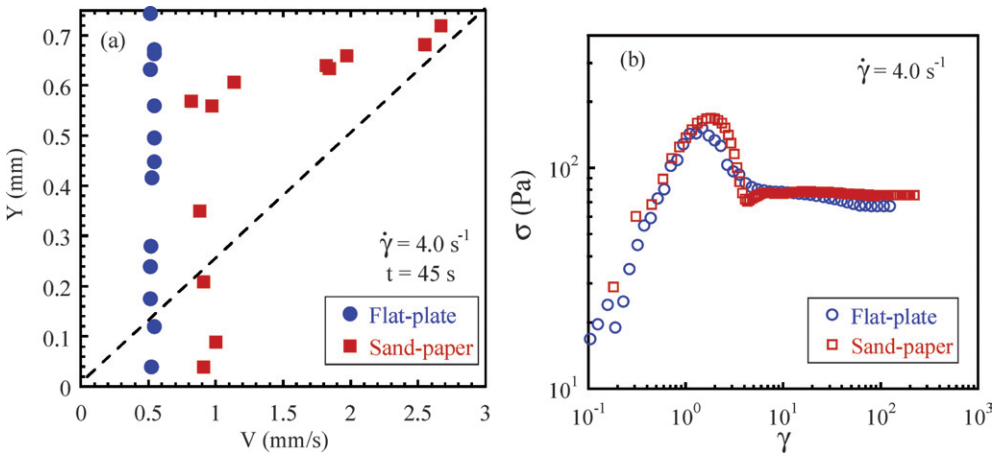

Fig. 17 (a) At apparent shear rate 4 s^{-1}, the sandpaper surface causes the shear inhomogeneity to invade into the sample interior whereas significant wall slip is still present at the flat surfaces. (b) The rheological measurements also show some difference.

more evident from the PTV observations at a higher applied rate of 4 s^{-1} as shown in Fig. 17(a) and (b). The sandpaper clearly allowed the sample to exhibit bulk shear inhomogeneity whereas the flat surface ensured that wall slip prevails.

4. Conclusion

We have investigated the flow behavior of strongly entangled DNA solutions based on three different solvents: water, ETG and glycerol. Massive wall slip occurs in the water-based DNA solution thanks to the small viscosity of water, making it difficult for our particle-tracking velocimetric (PTV) technique to explore any shear banding in the sample interior. Surface roughness is found to suppress wall slip, permitting bulk banding to be observed. Wall slip can also be reduced significantly in magnitude by replacing water with glycerol as the solvent. However, even for the glycerol-based DNA solution, wall slip can be a dominant feature until the applied Weissenberg number (apparent shear rate times the terminal relaxation time) exceeds a critical value on the order of $2b_{max}/H$, where b_{max} is the maximum slip length and H is a characteristic gap distance. Both controlled-rate and controlled-stress modes produce the same apparent rheological states, *i.e.*, the same steady-state flow curves. Yet, the PTV measurements show differences in the velocity profile. In all three samples, the trend is universal: as the discretely applied rate increases, each solution goes through terminal flow, slip-dominant plug-like flow and eventual bulk shear banding. Correspondingly, in a creep experiment with a sufficiently high stress, each solution progressively evolves from a state of full entanglement, to interfacial slip and shear banding in the sample interior. A combination of wall slip and shear banding is present at intermediate rates. These transformations from no-slip to slip and from slip to bulk banding can be depicted in a predictive manner as approximately verified by the PTV measurements. Strikingly, even creep cannot avoid shear inhomogeneity. Shear homogeneity is restored only at sufficiently high shear rates near the end of the stress plateau.

Acknowledgements

We appreciate the suggestion from one reviewer that we examine the surface roughness effect on flow responses. This work is

supported, in part, by a small grant for exploratory research and a regular grant from the National Science Foundation (DMR-0603951, DMR-0821697) and by a PRF grant from the American Chemical Society (#40596-AC7).

References

1 *Soft and Fragile Matter: Nonequilibrium Dynamics, Metastability and Flow*, ed. M. E. Cates and M. R. Evans, IOP, Bristol, U.K., 2000.
2 R. G. Larson, *The Structure and Rheology of Complex Fluids*, Oxford University, Oxford, 1999.
3 P. T. Callaghan, M. E. Cates, C. J. Rofe and J. B. A. F. Smeulders, *J. Phys. II*, 1996, **6**, 375.
4 R. W. Mair and P. T. Callaghan, *Europhys. Lett.*, 1996, **36**, 719.
5 M. M. Britton and P. T. Callaghan, *Phys. Rev. Lett.*, 1997, **30**, 4930.
6 M. M. Britton, R. W. Mair, R. K. Lambert and P. T. Callaghan, *J. Rheol.*, 1999, **43**, 897.
7 E. Fischer and P. T. Callaghan, *Europhys. Lett.*, 2000, **50**, 803.
8 J. B. Salmon, A. Colin, S. Manneville and F. Molino, *Phys. Rev. Lett.*, 2003, **90**, 228303.
9 J. B. Salmon, S. Manneville and A. Colin, *Phys. Rev. E*, 2003, **68**, 051503.
10 L. Becu, S. Manneville and A. Colin, *Phys. Rev. Lett.*, 2004, **93**, 018301.
11 Y. T. Hu and A. Lips, *J. Rheol.*, 2005, **49**, 1001.
12 M. R. Lopez-Gonzalez, W. M. Holmes and P. T. Callaghan, *Soft Matter*, 2006, **2**, 855.
13 L. Becu, S. Manneville and A. Colin, *Phys. Rev. Lett.*, 2003, **93**, 018301.
14 P. E. Boukany and S. Q. Wang, *Macromolecules*, 2008, **41**, 1455.
15 C. Y. D. Lu, P. D. Olmsted and R. C. Ball, *Phys. Rev. Lett.*, 2000, **84**, 642.
16 P. A. Vasquez, G. H. McKinley and L. P. Cook, *J. Non-Newtonian Fluid Mech.*, 2007, **144**, 122.
17 L. F. Rossi, G. McKinley and L. P. Cook, *J. Non-Newtonian Fluid Mech.*, 2006, **136**, 79.
18 L. Zhou, P. A. Vasquez, L. P. Cook and G. H. McKinley, *J. Rhol.*, 2008, **52**, 591.
19 K. Rehage and H. Hoffmann, *Mol. Phys.*, 1991, **74**, 933.
20 P. T. Callaghan, *Rheol. Acta*, 2008, **47**, 243.
21 P. D. Olmsted, *Rheol. Acta*, 2008, **47**, 283.
22 S. Manneville, *Rheol. Acta*, 2008, **47**, 301.
23 P. T. Callaghan and A. M. Gil, *Macromolecules*, 2000, **33**, 4116.
24 J. van der Gucht, M. Lemmers, W. Knoben, N. A. M. Besseling and M. P. Lettinga, *Phys. Rev. Lett.*, 2006, **97**, 108301.
25 W. M. Holmes, P. T. Callaghan, D. Vlassopoulos and J. Roovers, *J. Rheol.*, 2004, **48**, 1085.
26 P. Tapadia and S. Q. Wang, *Phys. Rev. Lett.*, 2006, **96**, 016001; P. E. Boukany and S. Q. Wang, *J. Rheol.*, 2007, **51**, 217; S. Ravindranath and S. Q. Wang, *Macromolecules*, 2008, **41**, 2663.
27 P. Tapadia, S. Ravindranath and S. Q. Wang, *Phys. Rev. Lett.*, 2006, **96**, 196001; S. Ravindranath and S. Q. Wang, *J. Rheol.*, 2008, **52**, 341.
28 S. Q. Wang, S. Ravindranath, P. Boukany, M. Olechnowicz, R. Quirk, A. Halasa and J. Mays, *Phys. Rev. Lett.*, 2006, **97**, 187801; S. Ravindranath and S. Q. Wang, *Macromolecules*, 2007, **40**, 8031.
29 S. Q. Wang, S. Ravindranath, Y. Wang and P. E. Boukany, *J. Chem. Phys.*, 2007, **127**, 064903.
30 Y. T. Hu, L. Wilen, A. Philips and A. Lips, *J. Rheol.*, 2007, **51**, 275.
31 P. E. Boukany, Y. T. Hu and S. Q. Wang, *Macromolecules*, 2008, **41**, 2644; P. E. Boukany and S. Q. Wang, *J. Rheol.*, 2009, DOI: 10.1122/1.3009299.
32 R. E. Teixeria, A. K. Dambal, D. H. Richter, E. S. G. Shaqfeh and S. Chu, *Macromolecules*, 2007, **40**, 2461.
33 S. Q. Wang, *Macromolecules*, 2007, **40**, 8684.
34 L. A. Archer, R. G. Larson and Y. L. Chen, *J. Fluid Mech.*, 1995, **301**, 133.
35 V. Mhetar and L. A. Archer, *Macromolecules*, 1998, **31**, 6639.
36 N. Pluktaveesak, S. Q. Wang and A. Halsa, *Macromolecules*, 1999, **32**, 3045.
37 S. G. Hatzikiriakos and J. M. Dealy, *J. Rheol.*, 1991, **35**, 497.
38 K. B. Migler, H. Hervet and L. Leger, *Phys. Rev. Lett.*, 1993, **70**, 287.
39 G. Massey, H. Hervet and L. Leger, *Eur. Phys. Lett.*, 1998, **43**, 83.
40 V. Mhetar and L. A. Archer, *Macromolecules*, 1998, **31**, 8607–8617.
41 P. E. Boukany and S. Q. Wang, *J. Rheol.*, 2006, **50**, 641.
42 S. Ravindranath and S. Q. Wang, *J. Rheol.*, 2008, **52**, 957.
43 J. Sanchez-Reyes and L. A. Archer, *Langmuir*, 2003, **19**, 3304.